ARTICLE

Received 00th January 20xx, Accepted 00th January 20xx

DOI: 10.1039/x0xx00000x

³¹P Spin-Lattice and Singlet Order Relaxation Mechanisms in Pyrophosphate Studied by Isotopic Substitution, Field Shuttling NMR, and Molecular Dynamics Simulation

David E. Korenchan, †a Jiaqi Lu, †a Mohamed Sabba, b Laurynas Dagys, b Lynda J. Brown, b Malcolm H. Levitt, b and Alexej Jerschow*a

Nuclear spin relaxation mechanisms are often difficult to isolate and identify, especially in molecules with internal flexibility. Here we combine experimental work with computation in order to determine the major mechanisms responsible for ^{31}P spin-lattice and singlet order (SO) relaxation in pyrophosphate, a physiologically relevant molecule. Using field-shuttling relaxation measurements (from 2 μ T to 9.4 T) and rates calculated from molecular dynamics (MD) trajectories, we identified chemical shift anisotropy (CSA) and spin-rotation as the major mechanisms, with minor contributions from intra- and intermolecular coupling. The significant spin-rotation interaction is a consequence of the relatively rapid rotation of the -PO $_3$ ²⁻ entities around the bridging P-O bonds, and is treated by a combination of MD simulations and quantum chemistry calculations. Spin-lattice relaxation was predicted well without adjustable parameters, and for SO relaxation one parameter was extracted from the comparison between experiment and computation (a correlation coefficient between the rotational groups).

Introduction

Nuclear spin relaxation holds a wealth of information about the dynamics of chemical systems. The main contributions to relaxation include chemical shift anisotropy (CSA), dipolar coupling interactions, paramagnetic interactions, and, for highly mobile molecules (especially in the gas phase), spin-rotation interactions.² Disentangling the relative contributions of each can be difficult, and the spin-rotation mechanism has been under-explored, especially in flexible molecules in solution.^{3, 4} Progress has been made recently in accurately computing relaxation rates with molecular dynamics (MD) simulations and *ab initio* calculations in small molecules and ions,⁵⁻⁹ and it has been demonstrated that very few (if any) adjustable parameters may be required in order to do so.⁹

Nuclear spin singlet order (SO) relaxation has been of particular interest, since it offers the opportunity of potentially achieving particularly long magnetization storage mechanisms (the SO relaxation time $T_{\rm S}$ has been shown in some cases to be up to two orders of magnitude larger than $T_{\rm 1}$). $^{10\text{-}18}$ As a result, SO relaxation can be diagnostic of particularly weak relaxation mechanisms. 9 The underlying reason is that the spin symmetry of such states can eliminate the strongest relaxation mechanisms. $^{19\text{-}22}$ The study of nuclear singlet order has led to

Very recently, ³¹P spin-lattice and SO relaxation have been studied in large diphosphate compounds.^{8, 39} For the ³¹P spins in the compounds studied, however, SO relaxation has been found to be more rapid than spin-lattice relaxation, with a major reason being the anticorrelation between the chemical shift anisotropy (CSA) tensors of the two spins.⁸

Two aspects of this prior work motivated us to examine ³¹P-spin relaxation further. The compounds used previously were particularly bulky and contained large asymmetries between the two spins (either transient or constant). We therefore sought to study the small, highly symmetric molecule pyrophosphate, modified to have slight asymmetry, thereby enabling access to SO. The molecule was further considered due to its physiological relevance. An additional aspect motivating this study was the proposal that ³¹P nuclear spin states could be of relevance in physiological processes, hypothesized to include cognition.⁴⁰

Since the main mechanism in prior work on substituted phosphates appeared to be due to CSA, we wished to perform magnetic field-dependent studies. We present here Zeeman and SO relaxation studies over a large field range (2 μT to 9.4 T) to investigate the major relaxation mechanisms as a function of magnetic field and determine the low-field limit to these relaxation rates. We further identify the mechanistic contributions to these relaxation rates by MD simulations and ab initio computation, and we demonstrate that both the CSA

Electronic Supplementary Information 1 available: [details of any supplementary information available should be included here]. See DOI: 10.1039/x0xx00000x

new applications in hyperpolarization,^{23, 24} contrast development for imaging,²⁵ measurement of slow processes such as molecular rearrangement,²⁶ diffusion,²⁷ and bond rotation,²⁸ the development of new pulse sequences,^{26, 29-36} and spectral editing.^{33, 37, 38}

^{a.} Department of Chemistry, New York University, 100 Washington Square E, New York. NY 10003.

b. School of Chemistry, University of Southampton, Southampton SO17 1BJ, UK.

[†] These authors contributed equally.

and spin-rotation contributions can be derived successfully from the simulations with only one adjustable parameter.

Results

Preparation and characterization of slightly chemically inequivalent pyrophosphate

One challenge in the study of SO in the pyrophosphate (PP_i) molecule is the lack of inequivalence (either chemical or magnetic), which is needed for creating and reading out SO of the ³¹P spins. To overcome this challenge, we unsymmetrically labeled PP_i with the ¹⁸O isotope. The increased mass of the ¹⁸O nuclei relative to the abundant 16O isotope was expected to induce a small chemical shift difference between the neighboring 31P nuclei, sufficiently large to allow creation and read-out of SO. This strategy was used previously for pairs of ¹³C nuclei.41 The tetrasodium salt of the unsymmetrically labelled ¹⁸O-PP_i (uPP_i) was synthesized and prepared in D₂O under highly alkaline conditions (for details, see Materials and Methods section) to avoid potentially interfering effects due to proton exchange, which can accelerate SO relaxation.⁴² The addition of 10 equivalents of potassium hydroxide (KOH) was found to promote longer SO lifetimes between the uPP_i ³¹P nuclei (Fig. S1, ESI). Similar results were obtained by adding ethylenediaminetetraacetate (EDTA) instead (Fig. S1, ESI).

The NMR properties of the synthesized uPP $_{\rm i}$ $^{31}{\rm P}$ spin system were extracted from a $^{31}{\rm P}$ pulse-acquire spectrum acquired at 9.4 T by multiplet simulation and fitting using the Spinach MATLAB package (http://spindynamics.org/group/). 43 Fig. 1 displays the fitting results. The unsymmetrical isotopic labelling of the uPP $_{\rm i}$ induces a slight chemical shift difference $\Delta\delta_{\rm PP}$ between the two $^{31}{\rm P}$ nuclei of 0.0663 ppm, or 10.7 Hz at 9.4 T. The $^{31}{\rm P}$ nuclei share a homonuclear *J*-coupling of magnitude $^{2}J_{\rm PP}$ = 21.5 Hz. Thus, the uPP $_{\rm i}$ $^{31}{\rm P}$ spin system is in a strongly coupled regime at 9.4 T. Singlet-triplet mixing can occur at high fields, but this mechanism of SO decay is eliminated when the sample is moved to lower fields. Additional peaks are observed which likely stem from partial labelling of the molecule. We could not

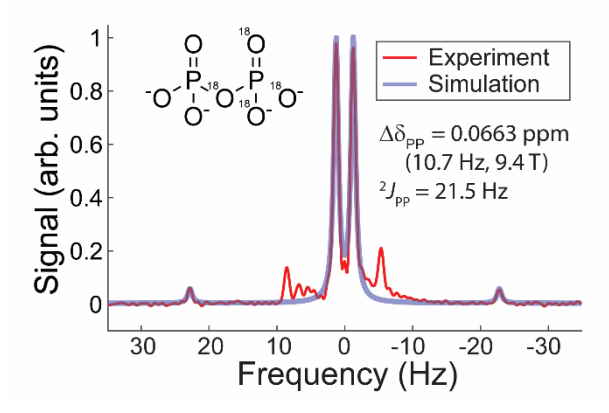


Fig. 1 $^{-31}$ P NMR spectrum and fitting results of fully deprotonated unsymmetrical pyrophosphate in KOH and D_2 O. Additional unidentified peaks arising from the synthesis besides the inner and outer doublet of doublet peaks were excluded from fitting. Fitted $^{-31}$ P chemical shift difference and homonuclear J-coupling values are displayed to the right of the spectra. The structure of the unsymmetric pyrophosphate is shown on the toplieft.

fully identify these, but products with partial labelling should not affect the results, since the triplet-singlet transfer is tailored to a particular chemical shift / coupling combination. The isotope composition should not affect relaxation rates due to the small differences in mass. The $^{31}P\,R_1$ values of the unlabeled PP_i and the ^{18}O -labeled uPP_i measured at 9.4 T were 0.107 s⁻¹ and 0.102 s⁻¹, respectively, with identical solution conditions (pD 14.4, 25 °C).

NMR field-cycling relaxation measurements of $\mbox{uPP}_{\mbox{\scriptsize i}}$

then performed 31**P** field-dependent relaxation measurements of both spin-lattice and SO relaxation, in order to compare and contrast known relaxation mechanisms. The spin lattice relaxation rate constant R_1 (= $1/T_1$) was measured using an inversion-recovery pulse sequence. For the measurement of the SO relaxation rate R_S (= 1/ T_S), we chose to utilize the spin-lock induced crossing (SLIC) pulse sequence³² for preparing and reading out SO for NMR spectroscopic relaxation measurements. Instrumentation details are described in the Materials and Methods section. The SLIC pulse sequence used for field-dependent measurements of R_S is displayed in Fig. 2. Optimization of the SLIC spin-lock pulse power and duration confirmed the spin system parameters determined via spectral fitting: the optimal pulse amplitude and duration corresponded with ${}^2J_{PP}$ of 20.3 Hz and a $\Delta\delta_{PP}$ of 12.3 Hz (Fig. S2, ESI).

The results of the relaxation measurements are shown in Fig. 3. Generally, the R_1 and R_5 values tracked each other, with R_1 experiencing a slight increase in the 2 μ T to 200 mT range. R_5 also tended to be smaller than R_1 in the high-field regime, above 4.5 T. Both R_1 and R_5 approached a constant relaxation rate offset of approximately 0.018 s⁻¹ at the lowest field values measured. The measured relaxation trends with magnetic field were well approximated using MD simulations and *ab initio* calculation (Fig. 3, dashed lines), as described below.

Molecular dynamics simulation and *ab initio* calculation of relaxation rate curves

In order to study the CSA tensors in uPP_I and their contributions to longitudinal and SO relaxation, MD simulations were performed using Gaussian 16 and Amber20⁴⁴ software, as described in the Materials and Methods section. Fig. 4 shows

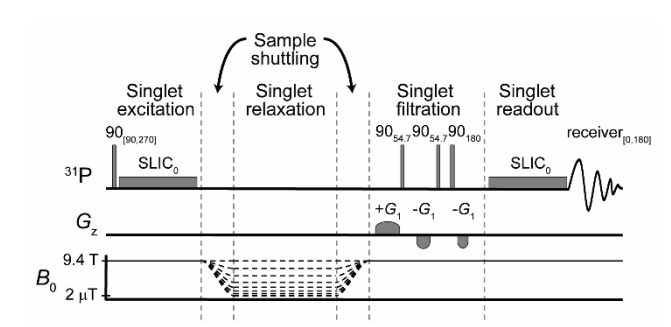


Fig. 2 Pulse sequence diagram for field-shutting singlet relaxation measurements using SLC pulses. Conversions between detectable magnetization and singlet order were performed at 9.4 T, and the sample was shuttled to owlfield for the incremented relaxation delay, then shuttled back for detection. A T_{00} filter prior to singlet readout was used with two-step phase cycling on the first 90° pulse and receiver to remove undesired coherence pathways.

Journal Name ARTICLE

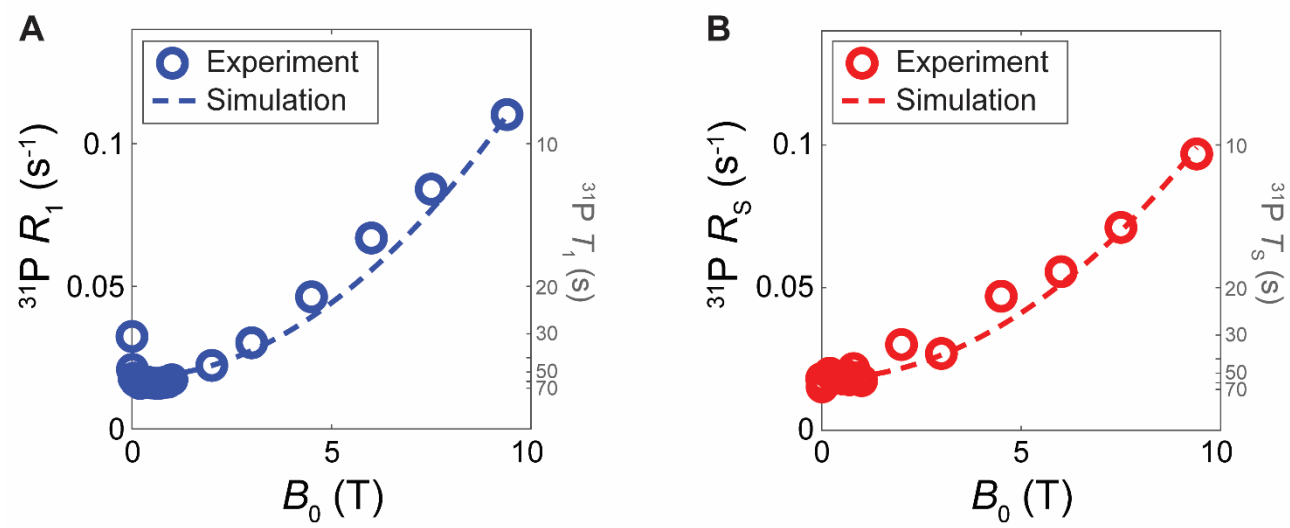


Fig. 3 31P NMR relaxation measurements of fully deprotonated 30 mM unsymmetrical pyrophosphate as a function of magnetic field strength (4) spin-attice relaxation, (B) SO relaxation Openic rices indicate experimental measurements, and dashed lines indicate the total simulated relaxation curve. For each plot, time constantivalues are shown on the right years with chicogrespond with the relaxation rate values on the left years.

average and multiple-snapshot representations of the symmetric portion of the CSA tensors experienced by the 31P nuclei. The CSA tensor visualizations show that the principal component appears almost completely aligned with the bond between phosphorus and the bridging oxygen. Because the $-PO_3^{2-}$ groups experience fast intramolecular rotation about the bridging P-O bond (see Fig. 4B), the CSA tensors were averaged across the 100 conformations, following molecular alignment along the P-P vector. A more detailed justification for this averaging procedure can be found in the Materials and Methods section. The difference between the average tensors at each 31P nucleus was computed, and the average and difference tensors were separated into their symmetric and antisymmetric components. The (Frobenius) norms of the tensor components are summarized in Table 1 and were used to calculate the CSA contributions to R_1 and R_S using the expressions

CSA tensor component	Norm of individual tensor averages (ppm)	Norm of difference tensor averages (ppm)
Symmetric	92.8	79.6
Antisymmetric	9.1	18.2

$$R_1^{sym} = \frac{2}{15} \left(\omega_0 \sqrt{\frac{3}{2}} \left\| \sigma_{sym} \right\|_F \right)^2 \frac{\tau_2}{1 + (\omega_0 \tau_2)^2}$$
 (1)

$$R_1^{anti} = \frac{1}{6} (\omega_0 || \sigma_{anti} ||_F)^2 \frac{\tau_1}{1 + (3\omega_0 \tau_1)^2}$$
 (2)

$$R_S^{sym} = \frac{2}{9} \left(\omega_0 \| \Delta \sigma_{sym} \|_F \right)^2 \frac{1}{5} \left(2\tau_2 + \frac{3\tau_2}{1 + (\omega_0 \tau_2)^2} \right) \tag{3}$$

$$R_S^{anti} = \frac{2}{9} (\omega_0 || \Delta \sigma_{anti} ||_F)^2 \frac{\tau_1}{1 + (3\omega_0 \tau_1)^2}.$$
 (4)

These expressions have been first given in Ref.⁴⁵ for the fast motion regime, and have later been provided outside of the fast motion regime in Ref.⁴⁶ in this form. In the equations above, ω_0

is the Larmor frequency, $\|\sigma\|_F$ and $\|\Delta\sigma\|_F$ indicate the Frobenius norms of the average and difference tensors, respectively, and τ_1 and τ_2 are the first- and second-rank correlation times, respectively, where $\tau_1=3\tau_2$ assuming isotropic rotational diffusion. The second-rank correlation time was determined to be 48.6 ps, based upon MD simulation following adjustment using the NMR-measured PPi diffusion coefficient, as described in the Materials and Methods section.

It is seen that CSA accounts for the major relaxation effect at high magnetic fields. The symmetric CSA component (Fig. 5, solid lines) contributes the most to R_1 and R_5 at high field strengths, whereas the antisymmetric contribution (Fig. 5, dotted lines) is relatively small for both but much larger for R_5 than it is for R_1 . Other smaller, yet significant relaxation contributions, largely field-independent, are described further below.

The spin-rotation contribution to R_1 was calculated as follows: From MD simulations, the correlation function $\overline{\omega(0)\omega(t)}$ for the angular rotation frequency of the -PO₃²- entity about the bridging P-O bond of PPi was calculated. An exponential fit was performed to this function, which yielded $\overline{\omega(0)^2}$ and the correlation time au_I . These values were determined as 3.1 rad²ps⁻² and 0.0255 ps, respectively. Gaussian 16 was used to compute the spin-rotation tensor for ³¹P in PP_i at the B3LYP/aug-cc-pVTZ level, which produced the value for $C_{\parallel}/2\pi$ = 4.424 kHz, for rotation around the bridging P-O vector, and roughly two equivalent values for the perpendicular rotation $C_{\perp}/2\pi$ = 1.095 kHz. The spin-rotation tensors are visualized in Fig. S3 in the ESI, which indicates that the major component of this tensor also points along the bridging P-O bond similar to the CSA tensor. Given that the motion perpendicular to the P-O bond can be assumed to be very small by comparison (see Fig. 4B, showing the superposition of conformers obtained from MD trajectories), we neglect this portion and calculate the spin-rotation relaxation rate constant by the expression

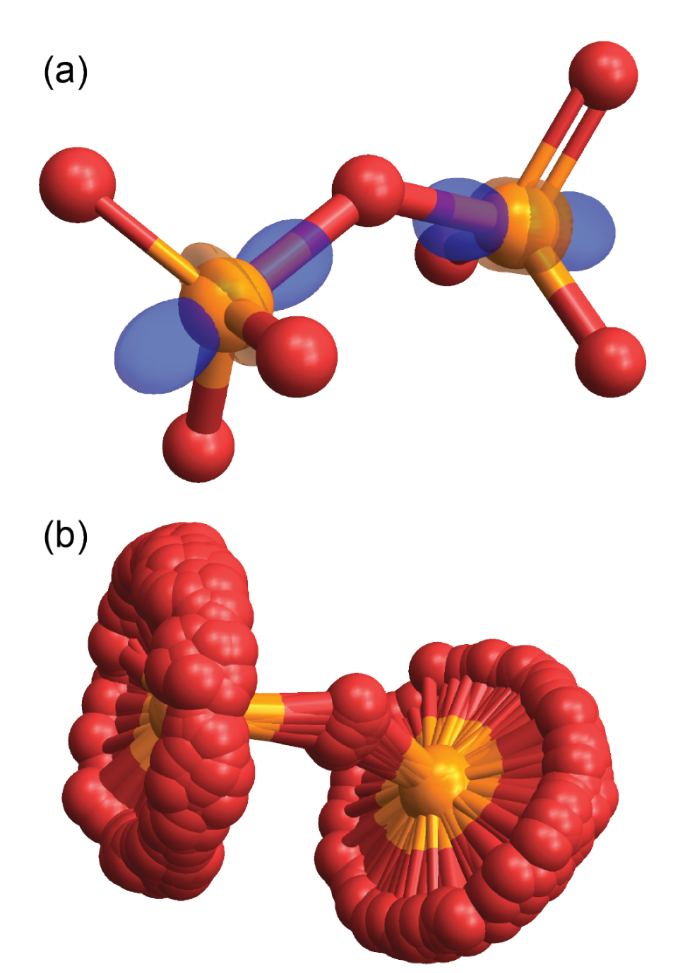


Fig. 4 Graphical representations of uPP_i molecular dynamics. **(A)** Ovaloid representation of the symmetric CSA tensor components experienced by each ³¹P nucleus. **(B)** Combined snapshots of conformations sampled by the uPP_i molecule within the molecular dynamics simulation, aligned along the P-P vector.

$$R_1^{SR} = \frac{2}{3\hbar^2} \overline{\omega(0)^2} I_{\parallel}^2 C_{\parallel}^2 \tau_J, \qquad (5)$$

where $I_{||}=1.758\cdot 10^{-45}$ kg m² is the moment of inertia for the -PO₃²- entity with respect to the bridging P-O axis. A derivation based on Pileio⁴7 and a consistency check with McClung⁴8 and Spiess⁴9 are provided in the ESI. The spin-rotation relaxation rate constant then becomes $R_1^{SR}=0.0113$ s¹. The rate is essentially independent of the magnetic field due to the extremely short correlation time for the angular frequency correlation function.

Spin-rotation is also expected to affect the relaxation of SO in uPP_i. We made the following considerations: were the spin-rotation field fluctuations produced by each rotating -PO₃²⁻ group fully uncorrelated, we would predict R_S^{SR} to be twice as large as R_1^{SR} . However, in this case R_S would be larger than R_1 at low field strengths, whereas experimentally we observed similar low-field values of R_1 and R_S . We therefore determined the correlation coefficient α for the spin-rotation interaction at each ³¹P spin following the discussion about correlated mechanisms of Tayler et al,⁵⁰ in particular Eqs. (1) and (2). From these considerations, one can obtain $R_S^{SR}/R_1^{SR} = 2(1-\alpha)$, as described in the derivation in the ESI. When using the experimental values for R_S^{SR} and R_1^{SR} we obtain the correlation

coefficient α = 0.5. Modelling the spin-rotation contribution to R_S in this manner produced an excellent fit to the experimental data (Fig. 3, dashed line). Other known relaxation contributions to R_1 and R_S are described below.

MD simulations following the procedure of Kharkov et al⁹ gave the contribution of intermolecular dipolar relaxation between ³¹P and ²D solvent spins as 5.14·10⁻³ s⁻¹. The ³¹P-³¹P dipolar relaxation contribution, relevant only for R_1 , was determined to be 1.60·10⁻³ s⁻¹. The correlation times for these processes range from 20-40 ps, and therefore their contributions are likewise almost completely independent of the magnetic field. The singlet-triplet leakage (STL) contribution to SO relaxation cannot easily be determined in closed form, since it depends on the specifics of the other relaxation mechanisms. This effect was therefore estimated using the Spinach NMR simulation package in MATLAB⁴³, by simulating SO relaxation with and without the chemical shift difference included and calculating the difference. The contribution is field-dependent but relatively minor, as seen in Fig. 5. Finally, the ¹H-³¹P dipolar relaxation contribution arising from the added KOH was estimated from the ²D-³¹P contribution as 0.00025 s⁻¹, which is negligible compared to other relaxation contributions.

Discussion

Our R_1 and R_S measurements show that uPP_i high-field relaxation is dominated by the CSA mechanism, similar to the case in other reported diphosphates.^{8, 39} In contrast to previous studies, however, the R_S values observed in the high field regime are slightly lower compared with R_1 . This finding corresponds well with the symmetric CSA tensor norm being somewhat lower for the difference tensor (Table 1). The norm of the antisymmetric component, however, is significantly larger for the difference tensors than for the individual tensors, with the result being a larger antisymmetric CSA contribution to R_S . Still, the antisymmetric contribution to R_S is smaller than one fifth of the symmetric contribution.

Importantly, we observed that towards low fields, a constant offset in the relaxation rate constants is approached for the experimentally measured values of both R_1 and R_5 . The offset at the lowest field, 2 μ T, was found to be approximately 0.018 s⁻¹ for both. The same trend and similar, albeit slightly higher R_1 and R_5 offsets were observed from measurements on a 30 mM uPP_i sample with 10 mM EDTA added (Fig. S4, ESI). We believe this constant contribution at the lowest field to be primarily comprised of spin-rotation relaxation, as shown in Fig. 5. Furthermore, at very low field strengths (2 μ T to 100 mT), R_1 showed a peculiar increase in the rate that was consistently observed across different sample formulations (Fig. S4A). This effect is not understood at this time.

Although our study was motivated by the biological relevance of pyrophosphate, we note that many of the experimental conditions used for our relaxation measurements are different from those that would be encountered in a biological system. First, our experiments were performed at a relatively high pD, to limit deuteron exchange. At physiological

Journal Name ARTICLE

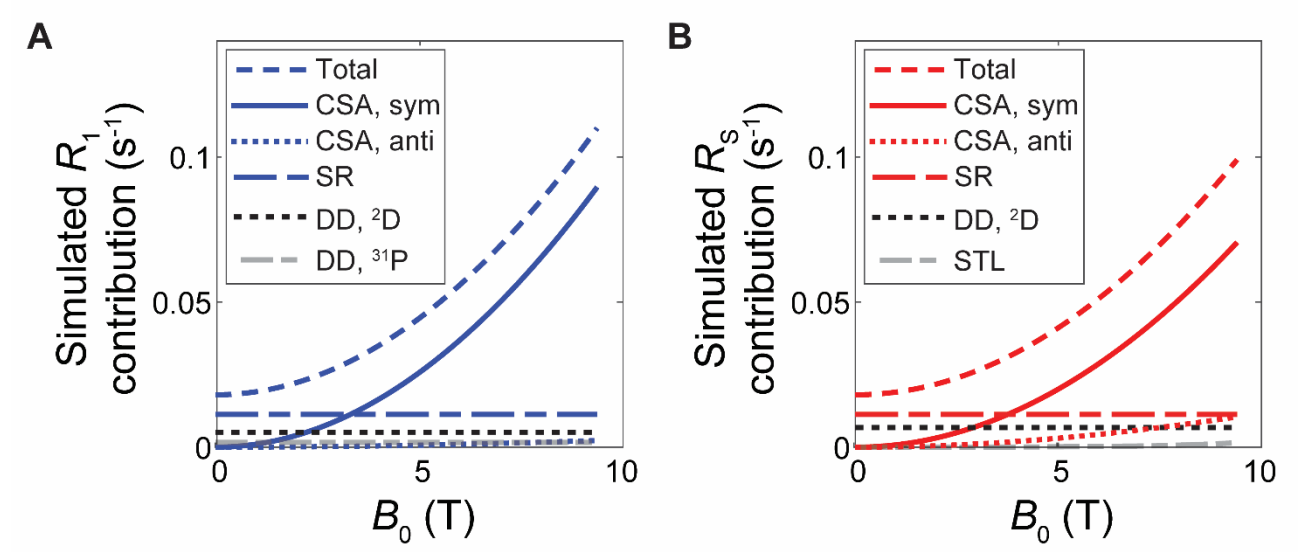


Fig. 5 Breakdo //n of totals mulated relaxation curre into components by relaxation mechanism. (A) calculated spin-lattice relaxation contributions, (B) calculated SO relaxation contributions. CSA = chemical shift an sotropy, SR = spin-rotation; DD = dipole-dip

pH values one can observe reduced T_S and T_1 relaxation times (similar to the case studied previously⁴²). In addition, the nature of the counterion might play a minor role in the relaxation measurements. Slightly longer T_1 times were observed when KOH was used in the uPP_i preparation, rather than NaOH (see ESI). Furthermore, D_2O was used as a solvent rather than H_2O . We note that if H₂O were used as a solvent, the lifetime limit would be significantly smaller. We measured an increase in R_1 of 0.028 $\ensuremath{s^{\text{-1}}}$ at 9.4 T when we replaced D_2O with 90% H_2O plus 10% D₂O. Assuming this increase to be field-independent, we would therefore expect a T_1 and T_S maximum of approximately 26 s for this solvent. Finally, certain paramagnetic species are abundant within cells and tissues and can contribute to relaxation. Comparison of rates observed in degassed and nondegassed samples, however, showed approximately the same rate constants in the low field region, suggesting that the effect of paramagnetic relaxation due to oxygen is low (Fig. S4, ESI). Other paramagnetic impurities were considered, but careful and extensive cleaning of glassware with KOH/iPrOH and HCl did not produce significant changes. Examination of relaxation in the presence of EDTA (to potentially capture paramagnetic impurities) likewise did not show significant changes in the observed rate constants (Fig. S4, ESI).

Conclusions

In summary, we report measurements of ^{31}P Zeeman magnetization and SO decay in isotope labeling-induced unsymmetric PP_i over a wide range of field strengths, with the largest values of the T_1 and T_5 time constants being approximately 65 s in the low field range. We demonstrate that CSA dominates both R_1 and R_5 relaxation at high fields and diminishes at low fields, and that the two rates have similar values from 2 μ T to 9.4 T. We observe that both R_1 and R_5 approach a constant value at low field strengths, which appears to be primarily explained by spin-rotation relaxation, with minor (but non-negligible) contributions from intermolecular $^{31}P^{-2}D$

dipolar coupling and intramolecular ³¹P-³¹P dipolar coupling. The magnitude of the spin-rotation relaxation contribution in this molecular system was an unexpected discovery, related to the relatively rapid rotation of the -PO₃²⁻ entities. In low magnetic fields the ³¹P singlet lifetime of pyrophosphate would possibly be long enough to sustain the entanglement of spin pairs in solution, and perhaps even mechanisms relevant for in quantum cognition.40,51 However, as far as the authors know, there is no evidence that cognition is significantly disturbed by high magnetic fields, as would be anticipated from the experimental results described here. Overall, these studies point to the importance of internal motions for the spinrotation relaxation mechanism in flexible molecules in solution for both spin-lattice, and SO relaxation, and also to the possibility of accurately predicting relaxation rates from MD simulations.

Materials and methods

Unsymmetrically $^{\rm 18}\textsc{O-labeled}$ pyrophosphate synthesis and formulation

The synthesis of ¹⁸O/¹⁶O unsymmetrical pyrophosphate tetrasodium salt 6, henceforth referred to as uPP_i, is shown in Fig. S5. Light sensitive silver phosphate salt 1 was prepared from ¹⁸O phosphoric acid by a simple precipitation method. ⁵² Subsequent benzylation in the presence of excess benzyl chloride provided the triester 2 in 75% yield.53 Heating triester 2 in the presence of one equivalent of sodium iodide in acetone accomplished selective mono-deprotection,53 and the resulting dibenzyl phosphate sodium salt 3 was converted to the tetrabenzyl ¹⁸O/¹⁶O pyrophosphate **4** by reaction with dibenzyl phosphoryl chloride (16O, obtained by the chlorination of dibenzyl phosphite with NCS in benzene and used directly)54 in the presence of triethylamine.55 Global debenzylation of the tetrabenzyl pyrophosphate using hydrogen over Pd required prolonged reaction times and was inefficient due to accompanying partial hydrolysis to the orthophosphate.

Ultimately, a two-step procedure via the dibenzyl pyrophosphate disodium salt $\bf 5$ was optimised, with the remaining two benzyl groups removed by hydrogenolysis over Pd in the presence of sodium bicarbonate in 5 hours. This six-step sequence afforded the regioselectively O^{18}/O^{16} labelled pyrophosphate tetrasodium salt $\bf 6$ as a white crystalline solid. Isotopic incorporation was confirmed by mass spectrometry to be 96% $^{18}O_4$, 96% $^{18}O_3$.

For NMR experiments, the tetrabasic sodium uPP_i was formulated as a 30 mM solution in deuterium oxide plus 10 equivalents of potassium hydroxide. The final concentrations of Na⁺ and K⁺ counterions were 120 mM and 300 mM, respectively. The pD of the solution was expected to be about 14.4, based upon room-temperature pH electrode measurements of a sample prepared identically but with unlabelled tetrabasic sodium pyrophosphate. The NMR tubes used with the samples were carefully cleaned to avoid any paramagnetic impurities by immersing in a KOH/iPrOH bath overnight followed by HCl immersion overnight, rinsing several times with acetone, and drying with argon gas. More details on sample preparation can be found in the ESI.

Field-dependent NMR spectroscopy

All field-dependent NMR measurements were performed at the University of Southampton, based on the design by Zhukov et al. 56 Approximately 300 μL of the uPP_i solution were placed in a 5 mm NMR tube and measured using a 9.4 T Bruker NMR spectrometer equipped with a home-built shuttling system, used to transport the sample rapidly between regions of different magnetic field. The shuttling system included a shielded region above the magnet and therefore enabled access to magnetic field strengths as low as 2 μ T. Spin-lattice relaxation was measured using an inversion-recovery sequence with magnetic field shuttling during the waiting time. SO was prepared with a spin-lock induced crossing (SLIC) spin-lock pulse³² at 9.4 T within the bore, the sample was shuttled to a region above the magnet for SO relaxation at the desired field strength, and then returned to the magnet bore for SO readout via SLIC (Fig. 1). The sample shuttling speed to and from the low field for all measurements was about 1 m/s, and the shuttling time (one-way) was no greater than 1 second. The sensitivity of singlet-triplet conversion due to transmitter offset during SLIC was mitigated by turning off the temperature regulation within the NMR scanner, in order to minimize the change in temperature between the bore and the shuttling region above the magnet. The probe temperature within the bore was measured to be about 22 °C with the temperature regulation off, and the temperature during sample shuttling was not expected to vary more than ±5 °C from the probe temperature.

Molecular dynamics simulations

MD simulations in Amber20 were performed as described previously²⁸ with the following modifications: PP_i was parametrized using ESP charges obtained from Gaussian 16 with B3LYP/6-31G(d), the polyphosphate parameters described by Meagher et al,⁵⁷ with the missing parameters provided by the GAFF2 force field. Minimization was performed in 5000 steps,

Timesteps were 1 fs throughout, and the isothermal/isobaric ensemble (NPT, 300 K, 1 bar) production run contained 107 steps. The simulation was performed at 300 K. 100 snapshots were selected randomly to perform ab initio calculations of CSA tensors with the B3LYP/aug-cc-pVTZ combination and the GIAO method. Fig. S6 in the ESI shows the individual tensor norms and eigenvalues of the tensor components for all conformers. To calculate the average CSA tensors across all selected conformations, the molecules were aligned along the P-P vector (i.e. along the x coordinate) with the bridging P-O vector pointing upwards in the x-z plane, as shown in Fig. 4B. The CSA tensors were rotated into this frame and averaged. For the R₁ calculation, the Frobenius norms were taken of the symmetric and antisymmetric components of the average tensors. For the R_S calculation, the Frobenius norm was calculated for the difference between the average tensors of each ³¹P. Tensor visualizations were generated using the Ovaloid function from SpinDynamica v3.658 in Mathematica, as described previously,^{59, 60} and displayed with MoleculePlot3D function.

The CSA tensor averaging procedure described above is strictly valid only in the limit where the internal motion is much faster than the overall tumbling rate. We justify its use as follows: from the MD trajectories the root mean square (rms) angular frequency of the -PO $_3^{2-}$ rotation around the bridging P-O bond is determined as 1.76 rad/ps. From this value, we can calculate the root-mean square rotation of -PO $_3^{2-}$ within the reorientation correlation time period determined above (48.6 ps) as 13.6 π . We therefore can assume that the -PO $_3^{2-}$ rotation is much faster than the molecular reorientation, so that averaging the tensors for the two $_3^{1}$ P spins prior to taking the differences between them is the correct approach.

The second-rank correlation time was extracted from the MD runs for the reorientation of the P-P bond, which was 65.4 ps. The diffusion of the pyrophosphate molecule was calculated from the MD trajectory as 0.215·10⁻⁹ m²/s. The experimental diffusion coefficient determined by pulsed-field gradient NMR was 0.37·10⁻⁹ m²/s (Fig. S7, ESI). Given the known relationships between rotational correlation times, diffusion coefficients, and viscosities, we therefore adjusted the correlation time obtained from computation by the factor 0.215/0.37, which resulted in a correlation time of 48.6 ps. This correlation time was further used in the spin dynamics simulations to obtain the relaxation rates.

Author Contributions

Conceptualization: AJ
Formal analysis: DEK, AJ
Funding acquisition: MHL, AJ
Methodology: DEK, JL, MS, LB, AJ
Project administration: MHL, AJ

Resources: LB

Investigation: DEK, JL, MS, LD, LB

Visualization: DEK, AJ

Journal Name ARTICLE

Supervision: LB, MHL, AJ Writing—original draft: DK, AJ

Writing—review & editing: DK, JL, LB, MHL, AJ

Conflicts of interest

There are no conflicts to declare.

Acknowledgements

D. E. K. thanks Christian Bengs and Jamie Whipham for helpful discussions regarding singlet NMR pulse sequences and NMR relaxation. The authors thank Alexey Kiryutin (International Tomography Centre, Novosibirsk, Russia) for sharing the shuttle design. This work was supported in part through the NYU IT High Performance Computing resources, services, and staff expertise (in particular by Dr Shenglong Wang).

Funding: National Science Foundation, award no. CHE 2108205 (AJ); Heising-Simons Foundation (AJ); Diamond Jubilee Visiting Fellowship, University of Southampton (AJ); EPSRC-UK, grant numbers EP/P009980/1, EP/T004320/1 and EP/P030491/1 (MHL); European Unions Horizon 2020 research and innovation programme, under the Marie Skłodowska-Curie grant agreement No 891400 (MHL); European Research Council, grant 786707-FunMagResBeacons (MHL).

Notes and references

- Yesinowski, J.P., R.J. Sunberg, and J.J. Benedict, pH control and rapid mixing in spinning NMR samples. Journal of Magnetic Resonance (1969), 1982. 47(1): p. 85-90.
- 2. Kowalewski, J. and L. Mäler, *Nuclear spin relaxation in liquids: theory, experiments, and applications.* 2018, Taylor & Francis Group, LLC. p. 1 online resource.
- 3. Lee, J.W., Spin-Rotation Interaction in Polyatomic Molecules in the Presence of Internal Rotation. Journal of the Korean Chemical Society, 1976. **20**(5): p. 364-373.
- 4. Håkansson, P., Prediction of low-field nuclear singlet lifetimes with molecular dynamics and quantum-chemical property surface. Physical Chemistry Chemical Physics, 2017. **19**(16): p. 10237-10254.
- 5. Odelius, M. and J. Kowalewski, *Molecular-Dynamics Simulation of Nuclear-Spin Relaxation of Li-7(+) in Water.*Journal of the Chemical Society-Faraday Transactions, 1995. **91**(2): p. 215-222.
- Rantaharju, J. and J. Vaara, Liquid-state paramagnetic relaxation from first principles. Physical Review A, 2016. 94(4): p. 043413.
- 7. Hakansson, P., Prediction of low-field nuclear singlet lifetimes with molecular dynamics and quantum- chemical property surface. Physical Chemistry Chemical Physics, 2017. **19**(16): p. 10237-10254.
- 8. Korenchan, D.E., et al., (31)P nuclear spin singlet lifetimes in a system with switchable magnetic inequivalence: experiment and simulation. Phys Chem Chem Phys, 2021. 23(35): p. 19465-19471.
- Kharkov, B., et al., Weak nuclear spin singlet relaxation mechanisms revealed by experiment and computation. Phys Chem Chem Phys, 2022. 24(12): p. 7531-7538.

- Carravetta, M., O.G. Johannessen, and M.H. Levitt, Beyond the T1 limit: singlet nuclear spin states in low magnetic fields. Phys Rev Lett, 2004. 92(15): p. 153003.
- 11. Carravetta, M. and M.H. Levitt, *Long-lived nuclear spin states in high-field solution NMR*. J Am Chem Soc, 2004. **126**(20): p. 6228-9.
- 12. Pileio, G., et al., Long-lived nuclear spin states in the solution NMR of four-spin systems. J Magn Reson, 2006. **182**(2): p. 353-7.
- 13. Sarkar, R., et al., Extending the scope of singlet-state spectroscopy. Chemphyschem, 2007. **8**(18): p. 2652-6.
- Pileio, G., et al., The long-lived nuclear singlet state of 15Nnitrous oxide in solution. J Am Chem Soc, 2008. 130(38): p. 12582-3.
- 15. Pileio, G., et al., Long-lived nuclear singlet order in near-equivalent 13C spin pairs. J Am Chem Soc, 2012. **134**(42): p. 17494-7.
- DeVience, S.J., R.L. Walsworth, and M.S. Rosen, Dependence of nuclear spin singlet lifetimes on RF spinlocking power. J Magn Reson, 2012. 218: p. 5-10.
- 17. Stevanato, G., et al., A nuclear singlet lifetime of more than one hour in room-temperature solution. Angew Chem Int Ed Engl, 2015. **54**(12): p. 3740-3.
- 18. Sheberstov, K.F., et al., Generating and sustaining long-lived spin states in (15)N,(15)N'-azobenzene. Sci Rep, 2019. 9(1): p. 20161.
- Levitt, M.H., Singlet and Other States with Extended Lifetimes, in Encyclopedia of Magnetic Resonance. 2010.
- 20. Levitt, M.H., *Singlet nuclear magnetic resonance*. Annu Rev Phys Chem, 2012. **63**: p. 89-105.
- 21. Levitt, M.H., et al., Long-lived Nuclear Spin Order: Theory and Applications. New Developments in NMR, ed. W.S. Price. Vol. 22. 2020: Royal Society of Chemistry.
- 22. Teleanu, F., A. Sadet, and P.R. Vasos, *Symmetry versus entropy: Long-lived states and coherences*. Prog Nucl Magn Reson Spectrosc, 2021. **122**: p. 63-75.
- Pileio, G., M. Carravetta, and M.H. Levitt, Storage of nuclear magnetization as long-lived singlet order in low magnetic field. Proc Natl Acad Sci U S A, 2010. 107(40): p. 17135-9.
- Pileio, G., et al., Recycling and imaging of nuclear singlet hyperpolarization. J Am Chem Soc, 2013. 135(13): p. 5084-8.
- 25. Pileio, G., et al., *Real-space imaging of macroscopic diffusion and slow flow by singlet tagging MRI.* J Magn Reson, 2015. **252**: p. 130-4.
- 26. Sarkar, R., P.R. Vasos, and G. Bodenhausen, Singlet-state exchange NMR spectroscopy for the study of very slow dynamic processes. J Am Chem Soc, 2007. **129**(2): p. 328-
- Cavadini, S., et al., Slow diffusion by singlet state NMR spectroscopy. J Am Chem Soc, 2005. 127(45): p. 15744-8.
- 28. Elliott, S.J., et al., Long-lived nuclear spin states in rapidly rotating CH2D groups. J Magn Reson, 2016. **272**: p. 87-90.
- 29. Kharkov, B., et al., Singlet excitation in the intermediate magnetic equivalence regime and field-dependent study of singlet-triplet leakage. Phys Chem Chem Phys, 2019. **21**(5): p. 2595-2600.
- Bengs, C., et al., Generalised magnetisation-to-singletorder transfer in nuclear magnetic resonance. Phys Chem Chem Phys, 2020. 22(17): p. 9703-9712.

- 31. Kharkov, B., et al., Effect of convection and B1 inhomogeneity on singlet relaxation experiments. J Magn Reson, 2017. **284**: p. 1-7.
- 32. DeVience, S.J., R.L. Walsworth, and M.S. Rosen, *Preparation of nuclear spin singlet states using spin-lock induced crossing.* Phys Rev Lett, 2013. **111**(17): p. 173002.
- 33. Kiryutin, A.S., et al., *Nuclear Spin Singlet Order Selection by Adiabatically Ramped RF Fields*. J Phys Chem B, 2016. **120**(46): p. 11978-11986.
- 34. Pravdivtsev, A.N., et al., Robust conversion of singlet spin order in coupled spin-1/2 pairs by adiabatically ramped RF-fields. J Magn Reson, 2016. **273**: p. 56-64.
- 35. Rodin, B.A., et al., *Using optimal control methods with constraints to generate singlet states in NMR.* J Magn Reson, 2018. **291**: p. 14-22.
- Pileio, G., Singlet NMR methodology in two-spin-1/2 systems. Prog Nucl Magn Reson Spectrosc, 2017. 98-99: p. 1-19.
- 37. Mamone, S., et al., *Singlet-filtered NMR spectroscopy*. Sci Adv, 2020. **6**(8): p. eaaz1955.
- 38. Devience, S.J., R.L. Walsworth, and M.S. Rosen, *Nuclear spin singlet states as a contrast mechanism for NMR spectroscopy*. NMR Biomed, 2013. **26**(10): p. 1204-12.
- 39. DeVience, S.J., R.L. Walsworth, and M.S. Rosen, *NMR of 31P nuclear spin singlet states in organic diphosphates.*Journal of Magnetic Resonance, 2021. **333**: p. 107101.
- Fisher, M.P.A., Quantum cognition: The possibility of processing with nuclear spins in the brain. Annals of Physics, 2015. 362: p. 593-602.
- 41. Tayler, M.C. and M.H. Levitt, *Accessing long-lived nuclear* spin order by isotope-induced symmetry breaking. J Am Chem Soc, 2013. **135**(6): p. 2120-3.
- 42. Bengs, C., et al., *Nuclear singlet relaxation by chemical exchange*. J Chem Phys, 2021. **155**(12): p. 124311.
- 43. Hogben, H.J., et al., Spinach--a software library for simulation of spin dynamics in large spin systems. J Magn Reson, 2011. **208**(2): p. 179-94.
- 44. Case, D.A., et al., *AMBER 2020*, in *AMBER 2020*. 2020, University of California, San Francisco.
- 45. Pileio, G., et al., Long-lived nuclear singlet order in nearequivalent 13C spin pairs. Journal of the American Chemical Society, 2012. **134**(42): p. 17494-17497.
- 46. Korenchan, D.E., et al., 31 P nuclear spin singlet lifetimes in a system with switchable magnetic inequivalence: experiment and simulation. Physical Chemistry Chemical Physics, 2021. **23**(35): p. 19465-19471.
- 47. Pileio, G., *Relaxation theory of nuclear singlet states in two spin-1/2 systems*. Progress in nuclear magnetic resonance spectroscopy, 2010. **56**(3): p. 217-231.
- 48. McClung, R.E.D., Spin-Rotation Relaxation Theory, in Encyclopedia of Magnetic Resonance. 2007.
- Spiess, H.W., Rotation of Molecules and Nuclear Spin Relaxation, in Dynamic NMR spectroscopy. 1978, Springer-Verlag: Berlin; New York. p. 214 p.
- Tayler, M.C. and M.H. Levitt, Paramagnetic relaxation of nuclear singlet states. Phys Chem Chem Phys, 2011. 13(20): p. 9128-30.
- 51. Weingarten, C.P., P.M. Doraiswamy, and M.P. Fisher, *A New Spin on Neural Processing: Quantum Cognition.* Front Hum Neurosci, 2016. **10**: p. 541.
- 52. Yan, T., et al., Fabrication of robust M/Ag3PO4 (M = Pt, Pd, Au) Schottky-type heterostructures for improved visible-

- *light photocatalysis.* RSC Adv., 2014. **4**(70): p. 37220-37230.
- Zervas, L. and I. Dilaris, Dealkylation and Debenzylation of Triesters of Phosphoric Acid. Phosphorylation of Hydroxy and Amino Compounds. J. Am. Chem. Soc., 1955. 77(20): p. 5354-5357
- 54. Gao, F., et al., Synthesis and Structure–Activity Relationships of Truncated Bisubstrate Inhibitors of Aminoglycoside 6'-N-Acetyltransferases. J. Med. Chem., 2006. **49**(17): p. 5273-5281.
- 55. Falck, J.R., et al., Synthesis and Structure of Cellular Mediators: Inositol Polyphosphate Diphosphates. J. Am. Chem. Soc., 1995. **117**(49): p. 12172-12175.
- Zhukov, I.V., et al., Field-cycling NMR experiments in an ultra-wide magnetic field range: relaxation and coherent polarization transfer. Physical Chemistry Chemical Physics, 2018. **20**(18): p. 12396-12405.
- 57. Meagher, K.L., L.T. Redman, and H.A. Carlson, Development of polyphosphate parameters for use with the AMBER force field. Journal of Computational Chemistry, 2003. **24**(9): p. 1016-1025.
- 58. Bengs, C. and M.H. Levitt, *SpinDynamica: Symbolic and numerical magnetic resonance in a Mathematica environment*. Magn Reson Chem, 2018. **56**(6): p. 374-414.
- 59. Radeglia, R., On the pictorial representation of the magnetic screening tensor: ellipsoid or ovaloid? Solid State Nucl Magn Reson, 1995. **4**(5): p. 317-21.
- 60. Young, R.P., et al., *TensorView: A software tool for displaying NMR tensors*. Magn Reson Chem, 2019. **57**(5): p. 211-223.